



Published in final edited form as:

*J Drug Target.* 2017 ; 25(9-10): 786–795. doi:10.1080/1061186X.2017.1349771.

## ICAM-1 Targeting, Intracellular Trafficking, and Functional Activity of Polymer Nanocarriers Coated with a Fibrinogen-Derived Peptide for Lysosomal Enzyme Replacement

Carmen Garnacho<sup>a</sup> and Silvia Muro<sup>b,c,\*</sup>

<sup>a</sup>Department of Normal and Pathological Histology and Cytology, University of Seville School of Medicine, Seville, Spain

<sup>b</sup>Institute for Bioscience & Biotechnology Research, University of Maryland, College Park, MD USA

<sup>c</sup>Fischell Department of Bioengineering, University of Maryland, College Park, MD USA

### Abstract

Enzyme replacement is a viable treatment for diseases caused by genetic deficiency of lysosomal enzymes. However, suboptimal access of enzymes to target sites limits this strategy. Polymer nanocarriers (NCs) coated with antibody against intercellular adhesion molecule 1 (ICAM-1), a protein overexpressed on most cells under disease states, enhanced biodistribution and lysosomal delivery of these therapeutics. Whether this can be achieved using more biocompatible ICAM-1-targeting moieties is unknown, since intracellular uptake via this route is sensitive to the receptor epitope being targeted. We examined this using polymer NCs coated with an ICAM-1-targeting peptide derived from the fibrinogen sequence. Scrambled-sequence peptide and anti-ICAM were used as controls. NCs carried acid sphingomyelinase (ASM), used for treatment of type B Niemann-Pick disease, and fluorescence microscopy was employed to examine cellular performance. Peptide-coated/enzyme NCs efficiently targeted ICAM-1 (22-fold over non-specific counterparts;  $B_{max}$  ~180 NCs/cell;  $t_{1/2}$  ~28 min), recognized human and mouse cells (1.2- to 0.7-fold binding vs. antibody/enzyme NCs), were efficiently endocytosed (71% at 1 h chase), and trafficked to lysosomes (30-45% of internalized NCs; 2 h chase). This restored lysosomal levels of sphingomyelin and cholesterol within 5 h chase (~95% of disease levels), similar to antibody-enzyme NCs. This fibrinogen-derived ICAM-1-targeting peptide holds potential for lysosomal enzyme replacement therapy.

### Keywords

ICAM-1 targeting; fibrinogen-derived peptide; polymer nanocarriers; enzyme replacement therapy; lysosomal storage diseases; Niemann-Pick disease; acid sphingomyelinase

---

\*Silvia Muro, 5115 Plant Sciences Building, College Park, MD 20742. Tel:+1-301-405-4777; muro@umd.edu.

### Declaration of Interest

The authors declare no conflict of interest.

## Introduction

The lysosomal disorders (LDs) are a group of about 60 different diseases caused genetic deficiency of components located in the lysosomal membrane or its lumen [1]. This leads to aberrant acidification, trafficking, and/or degradative processing of macromolecules within lysosomes in cells throughout the body [2]. Because of the central role of lysosomes in regulating cellular functions relative to degradation, signalling, autophagy, apoptosis, plasmalemma repair, vesicular trafficking, recycling, etc. [3], said lysosomal defects cause multi-dysfunctions that affect both peripheral tissues and the central nervous system [1,3]. Depending on the type and degree of the associated deficiency, as well as other epigenetic factors not fully understood, LD clinical onset ranges from the first months of life for highly severe conditions, to several years for milder syndromes [1,4]. Disease development is often rapid for neurological cases, which are typically fatal during the first months or years to life [1]. Slower progression associates with peripheral syndromes, whereby patients can develop to adulthood, yet these conditions are still highly debilitating and often lead to premature death [1].

Most LDs are particularly caused by defects affecting enzymes residing within the lysosomal lumen [1,4]. As such, these LDs associate with aberrant accumulation of the corresponding substrate in this compartment [1,4]. A clinically available treatment of these conditions is enzyme replacement therapy (ERT), where purified or recombinant enzymes are intravenously infused in patients approximately every two weeks [4,5]. Because these therapeutic enzymes are glycosylated and contain mannose-6-phosphate (M6P) residues, they can bind to the M6P receptor expressed on cells in the body [1,4]. This leads to endocytic uptake and trafficking to lysosomes of the administered enzyme, where the missing activity is replaced with attenuation of the corresponding storage. About a dozen different ERT products are approved and commercialized for human treatment and several more are under clinical trial, for a total of 8 LDs [4].

Despite this significant advance, several limitations remain which warrant further improvement. This include, among other, high enzyme uptake by the hepatosplenic system and lower uptake by other tissues, which is compensated by high and frequent enzyme dosing, leading to secondary side effects [4,5]. The facts that: (a) endocytic transport via the M6P receptor appears to be altered in some LDs, (b) the M6P receptor does not transport enzymes across endothelial cells in the blood-brain barrier, and (c) many biotechnological strategies do not render appropriate glycosylation or M6P display on recombinant enzymes, altogether hinder the potential of current ERT approaches [1,4]. Alternative strategies to improve delivery and effects of lysosomal enzymes are being explored, including (but not limited to) targeting of other cell-surface receptors and use of drug nanocarriers (NCs), which may help enhance endocytic uptake and lysosomal trafficking of these therapeutics [4,6].

Along with other alternative approaches, polymer NCs targeted to intercellular adhesion molecule 1 (ICAM-1) have shown to be highly promising toward this goal [4,7-9]. ICAM-1 is a transmembrane glycoprotein expressed on most cell targets in LDs, e.g., endothelial, epithelial, smooth and striated muscle, glial and neuronal, immune, and other cells [10]. Its

expression is highly upregulated by numerous pathological factors such as metabolic imbalance, oxidative stress, inflammation, etc., often characteristic of LDs [10]. ICAM-1 associates to vesicular transport via the cell adhesion molecule (CAM)-mediated pathway, an endocytic mechanism independent from classical clathrin, caveolae, phagocytosis or macropinocytosis mediated routes [11,12], which remain active under LDs [13]. ICAM-1 targeting has been explored for diagnostic and therapeutic purposes in the context of metabolic, cardiovascular, inflammatory, cancer, and other conditions using conjugates, liposomes, dendrimers, micelles, nanoparticles, etc. [14-23].

Our previous studies on lysosomal ERT applications have shown significant potential of ICAM-1-targeted polymer NCs, as illustrated in the examples of acid sphingomyelinase (ASM) used for type B Niemann-Pick disease (NPD) [9,24],  $\alpha$ -galactosidase used for Fabry disease [8,25], and  $\alpha$ -glucosidase used for Pompe disease [7]. ICAM-1-targeted polymer NCs (both non-degradable polystyrene models and clinically-relevant poly(lactic-co-glycolic acid) (PLGA) NCs) were shown to markedly improve targeting and biodistribution of lysosomal enzymes in mice, and enhance their endocytosis and lysosomal trafficking in cells, with attenuation of storage in both models [7-9,26]. In these studies, however, ICAM-1 targeting was achieved by coating NCs with anti-ICAM antibody molecules and whether similar ERT efficacy can be obtained by using targeting moieties more amenable toward clinical applications (e.g., peptides), remains to be investigated. Although *a priori* one would expect this to be the case for any ICAM-1-targeting entity, it is not obvious for this particular application because: (a) CAM-mediated signaling and endocytosis has been shown to be highly sensitive to the specific receptor epitope being targeted [27,28], and (b) the presence of specific enzyme cargo capable of targeting the M6P receptor [2] may modulate the targeting ability of peptide-coated NCs. Therefore, the efficacy of a peptide/enzyme NC system must be empirically tested, which constituted the focus on the present study.

## Methods

### Materials

ICAM-1-targeting  $\gamma$ 3 peptide, whose sequence is derived from amino acids 117-133 of the fibrinogen gamma chain (NNQKIVNLKEKVAQLEA) [29], and a scrambled sequence peptide ( $\gamma$ 3S) were synthesized by GenScript (Piscataway, NJ). Monoclonal antibodies to human ICAM-1 were R6.5, purified from its corresponding hybridoma (American Type Culture Collection, Manassas, VA), and commercial antibody LB2 (Santa Cruz Biotechnology, Santa Cruz, CA). Non-specific IgG and secondary antibodies were from Jackson ImmunoResearch (West Grove, PA). Texas Red dextran (10 000 MW) and BODIPY-FL<sub>C12</sub>-sphingomyelin were from Molecular Probes (Eugene, OR). Fluoresbrite®-labeled polystyrene nanoparticles (100 nm diameter) were purchased from Polysciences (Warrington, PA). Poly(D,L-lactide co-glycolide) (PLGA) was from Lakeshore Biomaterials (Birmingham, AL). Na<sup>125</sup>I was from Perkin Elmer (Waltham, MA) and Iodogen from Pierce Chemical (Rockford, IL). Recombinant human ASM was kindly provided by Dr. Edward Schuchman (Department of Genetics and Genomic Sciences, Mount Sinai School of Medicine, New York, NY). Cell media and supplements were from Cellgro (Manassas, VA)

and Gibco BRL (Grand Island, NY). Unless otherwise stated, all other reagents were from Sigma-Aldrich (St. Louis, MO).

### Nanocarrier preparation

Commercial 100 nm diameter, green Fluoresbrite®-labeled or non-labeled polystyrene nanoparticles were used as model NCs. Functional results were validated using PLGANanoparticles, which were prepared using nanoprecipitation with solvent evaporation [24,26,30]. For this, an organic phase of 20 mg/ml PLGA in acetone (50:50 copolymer ratio and 32 kDa molecular weight) was added under agitation into filtered deionized water at a 1:10 dilution. The emulsion was stirred for 16 h at room temperature to evaporate the organic solvent and the NC suspension was then filtered, dialyzed, and concentrated using a rotary evaporator. Following established methods [30-32], a suspension of  $10^{10}$  particles/ $\mu$ L polystyrene or PLGA NCs were coated by surface adsorption with 300 nM recombinant ASM and 3 nM ICAM-1-specific  $\gamma$ 3 peptide or non-specific  $\gamma$ 3S control ( $\gamma$ 3/ASM NCs and  $\gamma$ 3S/ASM NCs, respectively), or with 5  $\mu$ M ASM and 2.5  $\mu$ M anti-ICAM antibody R6.5 (anti-ICAM/ASM NCs) [9,24]. Where indicated, ASM was pre-labelled with  $^{125}$ Iodine to quantify loading of this therapeutic cargo on the NC surface using  $^{125}$ I-ASM specific activity and a gamma-radiation counter (Wizard<sup>2</sup>; PerkinElmer) [9]. Non-coated proteins were removed by centrifugation and coated NCs were resuspended at  $\approx 10^9$  NCs/ $\mu$ L in 1% bovine serum albumin (BSA)-supplemented phosphate buffered saline (PBS) and sonicated [31]. The enzyme loading efficiency was calculated as the enzyme that coated nanoparticles (recovered in the pellet) compared to the total amount of enzyme added to the coating reaction, expressed as a percentage. The absolute amount of enzyme coated per nanoparticles was calculated from the amount of  $^{125}$ Iodine in the nanoparticle pellet, the measured  $^{125}$ Iodine cpm per mass of enzyme, and the known number of nanoparticles in the coating mixture, as previously described [31]. The diameter of the resulting NCs, the polydispersity index (PDI), and the Z potential were determined by dynamic light scattering (Zetasizer NanoZS90, Malvern Instruments, Westborough, MA, USA).

### Cell culture

Human umbilical vein endothelial cells (HUVECs; Clonetics, San Diego, CA) or mouse microvascular-epithelial hybrid H5V cells were seeded on 1% gelatin-coated glass coverslips and activated for 16 hours with 10 ng/ml tumor necrosis factor  $\alpha$  (TNF $\alpha$ ; BD Biosciences, Franklin Lakes, NJ) to mimic the inflammatory state in NPD. Cells were cultured using M-199 and Dulbecco's modified Eagle's medium (DMEM), respectively, both supplemented with fetal bovine serum, glutamine, growth factors, and antibiotics as previously described [8]. Skin fibroblasts from normal individuals or NPD patients (a gift from Dr. Edward Schuchman, Department of Genetics and Genomic Sciences, Mount Sinai School of Medicine, New York, NY) were grown on similar coverslips, without the addition of TNF $\alpha$ , and in similarly supplemented DMEM, as reported [24].

### NC binding to cells

TNF $\alpha$ -activated HUVECs or H5V cells (fixed to avoid uptake or live as a more physiological condition, as specified in respective figure legends) incubated between 5 min and 3 h at 37°C with specific  $\gamma$ 3/ASM- vs. non-specific  $\gamma$ 3S/ASM-coated green

Fluoresbrite®-polystyrene NCs. For a comparison, cells were similarly incubated with anti-ICAM/ASM NCs. Incubations were conducted in control medium or medium containing binding competitors, including: (a) M6P, which binds to the M6P receptor recognized by ASM, or (b) anti-ICAM antibody LB2, which binds to ICAM-1 on the same domain recognized by  $\gamma 3$ . Non-bound NCs were then washed off, cells were fixed, and samples were imaged by phase-contrast and fluorescence microscopy using an Eclipse2000-U fluorescence microscope (Nikon, Melville, NY), a 60X PlanApo objective, and a FITC filter. Images were taken using an ORCA-1CCD camera (Hamamatsu Corporation, Bridgewater, NJ) and analyzed using Image-Pro 6.3 software (Media Cybernetics, Bethesda, MD), to quantify the number of NC bound per cell. This is automatically assessed using a previously described algorithm that detects and counts fluorescent objects whose pixel size is equivalent that of NCs and which amply surpass the fluorescence intensity of the surrounding background [31].

### NC endocytosis by cells

TNF $\alpha$ -activated HUVECs were incubated for 1 h at 37°C (pulse) with  $\gamma 3$ /ASM green Fluoresbrite®-polystyrene NCs containing tracer amounts of non-specific IgG. NCs that did not bind to cells within this time were washed off and cells were incubated for 1 h at 37°C in NC-free medium to permit internalization of pre-bound NCs (chase). Similar experiments were conducted in presence of 3 mM amiloride to inhibit CAM-mediated endocytosis, or 1  $\mu$ g/ml filipin to inhibit caveolae-mediated uptake. Cells were washed, fixed, and incubated with Texas Red-labeled goat anti-mouse IgG, which can bind to tracer IgG on the NC coat only if NCs are located on the cell surface, not if they are internalized within cells. This enables differential visualization of cell surface-bound NCs as yellow objects (green + red) vs. internalized counterparts which appear green [31]. Samples were imaged by phase-contrast and fluorescence microscopy to quantify the percentage of internalized NCs from the total number of NCs associated to cells, as described [31].

### Lysosomal trafficking of NCs

TNF $\alpha$ -activated HUVECs or H5V cells were first incubated for 1 h at 37°C with Texas Red dextran, which has previously demonstrated to traffic to lysosomes in these cells [33]. Then, cells were washed and incubated for 1 h at 37°C with either  $\gamma 3$ /ASM- or anti-ICAM/ASM-coated green Fluoresbrite®-polystyrene NCs (pulse). Non-bound NCs were washed off and incubations were continued in NC-free medium for 2 h to enable bound NCs to traffic intracellularly (chase). Cells were washed, fixed, and imaged by phase-contrast and fluorescence microscopy to quantify the percentage of green NCs colocalizing with red-labeled lysosomes, as described [24].

### Therapeutic activity of NCs

Skin fibroblasts from normal (wild type) individuals or NPD patients were incubated overnight with 0.2  $\mu$ g/mL BODIPY-FL<sub>C12</sub>-sphingomyelin to enable storage of this fluorescent lipid in these ASM-deficient cells, as described [24]. Cells were then washed and incubated for 1 h pulse at 37°C with control medium vs. medium containing  $\gamma 3$ /ASM polystyrene NCs or  $\gamma 3$ /ASM PLGA NCs, then washed and incubated for additional 5 h in the absence of NCs, to enable pre-bound NCs to traffic to lysosomes. After this, cells were

washed, fixed, and cholesterol storage was stained blue with 10  $\mu\text{g}/\text{ml}$  filipin [13]. Fluorescence microscopy was then used to quantify the level of red-sphingomyelin and blue-cholesterol in NC-treated cells and this was expressed as a percentage of the corresponding levels in untreated cells, as described [13,24].

## Statistics

Data were calculated as the mean  $\pm$  standard error of the mean (SEM) for  $n = 3$  experiments, where statistical significance was determined by Student's *t*-test.

## Results

### Design and characterization of model peptide-targeted NCs

To first focus on targeting as well as endocytic and lysosomal transport questions, we first used model NCs consisting of fluorescent polystyrene nanoparticles, as in previous works [7,8,24,31]. While this material is non-degradable and holds little clinical significance, we have previously demonstrated that it represents a good model for mechanistic studies on the CAM pathway in cell cultures and *in vivo* because ICAM-1 targeting, signaling and vesicular transport of antibody-targeted polystyrene models were same than for biodegradable PLGA counterparts [9,26], where NC geometry and targeting valency (not polymer itself) ruled these processes [15,31,34]. Instead, polystyrene models allow us to discern targeting and transport parameters without confounding results of simultaneous polymer degradation [31]. Hence, we started our study by using this model and then validated intralysosomal functional outcome, which requires binding, uptake and lysosomal trafficking using PLGA NCs.

Model NCs were coated by surface adsorption with targeting moieties and enzyme cargo. Targeting moieties were either  $\gamma 3$  peptide or anti-ICAM monoclonal antibody R6.5, for a comparison.  $\gamma 3$  is a 17-mer peptide derived from the sequence of a natural ICAM-1 ligand, fibrinogen [29]. Because fibrinogen is highly abundant in the circulation and  $\gamma 3$  is a short peptide without tertiary structure, this represents a biocompatible ICAM-1 targeting tool. A peptide of scrambled sequence ( $\gamma 3S$ ) was alternatively used, as a non-specific control. As per an enzyme cargo, we selected ASM (the enzyme deficient in types A-B NPD) since our previous studies on anti-ICAM/ASM NCs [9,24] provide a good historical control for new peptide-targeted NCs to be examined here. Surface-loading of lysosomal enzymes on NCs is a reasonable strategy because: (a) these enzymes are not intrinsically toxic as classical drugs are, but otherwise endogenous to the body and required ubiquitously in most tissues [1], (b) they are only active at acidic lysosomal pH and can be considered pro-drugs until the lysosome is reached [2], (c) presence of the NC surface provides fast intralysosomal activity without minute control of release required for encapsulated counterparts [8], and (d) this design has shown promising targeting, uptake, lysosomal trafficking, and enzyme activity with storage reduction in our previous works [7-9,13,24,25]. With regard to surface adsorption as a coating strategy, this results in random distribution of cargo and targeting moieties on the NC surface, which is no different from most strategies of covalent linkage where the exact position of the protein (antibody, peptide, enzyme) residue that is modified in each one protein molecule are not controlled. Just as the case of protein adsorption on a

plastic surface, e.g., for ELISA, protein adsorption on the NC surface has been shown to be relatively stable, including the presence of serum and physiological temperature, rendering high targeting *in vivo* [7-9].

As shown in Table 1, pristine non-coated polystyrene NCs had 117 nm hydrodynamic diameter, 0.07 PDI, and  $\zeta$ -potential of  $-37$  mV. Coating with both  $\gamma 3$  and ASM lead to an increase in the average diameter (209 nm) and (0.14 PDI), and less negative  $\zeta$ -potential ( $-25$  mV), as expected. This increase in the size and PDI was similar for non-specific  $\gamma 3$ S/ASM NCs (205 nm diameter and 0.19 PDI), and anti-ICAM/ASM counterparts (216 nm diameter, 0.14 PDI, and  $\zeta$ -potential of  $-27$  mV). Both peptide and antibody coated NCs contained a similar enzyme load (212 and 236 ASM molecules per NC) and the coating efficacy, calculated as the percentage of enzyme coated over the total amount of enzyme added to the coating mixture, was similarly high (80-85%).

### Binding of $\gamma 3$ /ASM NCs to cells

Using this polystyrene model, we next aimed to examine the targeting specificity and kinetics of  $\gamma 3$ /ASM NCs. Given the vascular endothelium represents one of the first layers of cells encountered after intravenous administration of lysosomal ERTs, which is both in need of therapy and at the interface between the blood and the surrounding tissues, we focused on this cell type for which we have historical controls [9,24].

As shown in Figure 1, binding of  $\gamma 3$ /ASM NCs to fixed endothelial cells (which had been activated to mimic the inflammatory state in LDs and also fixed to avoid NC uptake) was fast and efficient, with  $B_{max}$  of a 180 NCs bound per cell and a  $t_{1/2}$  of 28 min. Binding was highly specific, since control  $\gamma 3$ S/ASM NCs showed no significant binding to these cells, e.g., less than 10 NCs per cell after 3 h incubation, the maximal time point tested. Further confirming specificity (Figure 2), the presence of an anti-ICAM antibody (clone LB2), which is known to block the ICAM-1 binding site of fibrinogen, markedly hindered targeting of  $\gamma 3$ /ASM NCs (55% decrease at 30 min). This was not affected in the presence of M6P (105% of control binding), which should block binding of recombinant ASM to M6P receptors on cells [2].

In addition, we directly compared the targeting efficiency of  $\gamma 3$ /ASM NCs to that of anti-ICAM/ASM counterparts, both in human (HUVECs) and mouse (H5V) endothelial cells (Figure 3). In this case cells were live instead of fixed, to also estimate binding under more physiological conditions. In human cells,  $\gamma 3$ /ASM NCs showed somewhat enhanced binding as compared to anti-ICAM/ASM NCs (20% enhancement at 1 h) while binding to mouse cells was decreased (30% decrease vs. anti-ICAM/ASM NCs at that time; antibody clone YN1 was used instead of R6.5 to target mouse ICAM-1). Nevertheless, targeting of mouse endothelial cells was rather significant, as it resulted in  $\approx 50$  NCs bound per cell at 1 h vs. 5 NCs/cell found for control  $\gamma 3$ S/ASM NCs (not shown).

Therefore, results in this section show specific and efficient targeting of ICAM-1 by peptide-coated NCs, in pair with antibody-coated counterparts, which shall be useful to enhanced delivery of ASM delivery for NPD therapy.

## Endocytosis and lysosomal trafficking of $\gamma$ 3/ASM NCs

Subsequent to binding to target cells, endocytic uptake followed by lysosomal trafficking is required for effective lysosomal ERT delivery [1,2]. Therefore, we next examined the efficacy and mechanism of uptake of  $\gamma$ 3/ASM NCs, using endothelial cells as models (Figure 4). We employed a pulse-chase mode of incubation, where NCs were first allowed to bind to cells for 1 h (pulse), to reach binding saturation as established in previous results (Figure 1), and then non-bound NCs were washed and cell were incubated in NC-free medium for an additional hour (chase). This renders more synchronized endocytosis of pre-bound NCs and enables more accurate examination of the uptake efficacy vs. continuous incubation where both binding and uptake concomitantly happen. We also employed a dual-labeling technique previously established [11,31], where green-fluorescent NCs are used and those bound on the cell surface are counterstained after fixation with an antibody-labeled in a red fluorophore. Since cells are fixed, no further uptake is possible and, hence, surface-bound NCs appear double-labeled in green and red (yellow in merged images), while internalized NCs are single-labeled in green (Figure 4A). Differential microscopy quantification of these labels showed that  $\gamma$ 3/ASM NCs were efficiently internalized by cells, i.e.  $\approx$ 70% of all cell-associated NCs were located within cells after only 1 h chase time (Figure 4B). In addition, amiloride, which is a drug that inhibits the sodium-proton exchanger NHE1 involved in CAM-mediated endocytosis, significantly hindered NC uptake (53% reduction) while filipin, an inhibitor of unrelated caveolae-mediated transport used as a control, did not affect this (8% decrease).

With regard to lysosomal trafficking of  $\gamma$ 3/ASM NCs, this was assessed in parallel by colocalizing green-labeled NCs with red-labeled dextran (yellow color in merged images; Figure 5A). Dextran is a polysaccharide rapidly internalized and trafficked to lysosomes through the macropinocytic route, which cannot be degraded within mammalian lysosomes. Therefore, dextran can be used to trace lysosomal compartments regardless of their luminal pH, as previously verified [33]. Worth noticing is the fact that the green fluorophore that labels NCs is not pH sensitive and, additionally, lysosomal pH is neutral in fixed cells, avoiding potential imaging artifacts. A significant level of colocalization of  $\gamma$ 3/ASM NCs and lysosomes was found in both human and mouse endothelial cells, i.e. 25% of all NCs associated to human cells and 33% of those associated to mouse cells, by 2 h chase. Since parallel experiments similar to those shown in Figure 4 indicated that  $\approx$ 75-80% of NCs were inside cells at this time (not shown), this represents over 30-45% colocalization of internalized NCs with lysosomes (Figure 5B). This was similar to anti-ICAM/ASM NCs, which showed 35% lysosomal colocalization of all cell-associated NCs (not shown) and  $\approx$ 40% lysosomal colocalization of internalized NCs (Figure 5B), as in our previous studies [33].

Altogether, the results from this section indicate that significant endocytic uptake and lysosomal trafficking of  $\gamma$ 3/ASM NCs, ruled by mechanism and kinetics similar to that of antibody-coated counterparts.

### Therapeutic attenuation of lysosomal storage by $\gamma$ 3/ASM NCs

Ultimately, delivery of ASM to lysosomes is expected to result in a replacement of the missing enzymatic activity in patient cells, with therapeutic reduction of the corresponding lysosomal storage associated to disease. In the case of ASM-deficient NPD, the phospholipid sphingomyelin constitutes the primary storage in disease cells, since this is the substrate that ASM hydrolyzes [35]. Secondly, due to affinity between sphingomyelin and cholesterol, this lipid also accumulates in NPD. Therefore, we examined the ability of  $\gamma$ 3/ASM NCs to reduce sphingomyelin and cholesterol storage upon lysosomal delivery in cells (Figure 6A). In this case we used skin fibroblasts isolated from a NPD patient vs. a normal individual used as a wild type control. Verifying previous results, differential fluorescence labeling of sphingomyelin (red) and cholesterol (blue) showed 5-fold and 4.5-fold increase, respectively, in the levels of these lipids in diseased cells (compare “untreated” bars with the solid horizontal lines corresponding to the normal control in Figure 6B-C), with specific accumulation as punctate objects, indicative of lysosomal storage vs. cell-surface (which would appear diffuse on the plasmalemma), characteristic of NPD. Importantly, incubation with  $\gamma$ 3/ASM NCs for only 1 h binding pulse and then 5 h chase in NC-free medium to allow pre-bound NCs to traffic, fully eliminated the storage of both sphingomyelin and cholesterol, i.e. 93.6% and 94.9% reduction, respectively, compared to untreated diseased cells (Figure 6B). As a comparison, as our previous studies [13,24], anti-ICAM/ASM NCs reduced 89% sphingomyelin and 66% cholesterol storages after 1 h pulse + 4 h chase incubation (compare “untreated” bars with the dashed horizontal line corresponding to anti-ICAM/ASM NC treatment in Figure 6B-C), hence similar to  $\gamma$ 3/ASM NCs studied here.

Furthermore, since the model NCs used for these experiments consisted of non-degradable polystyrene, we verified our functional data using clinically-relevant PLGA counterparts (Figure 6). Since the storage reduction efficacy of NCs depends upon their binding, endocytosis, and lysosomal trafficking, a similar functional result for PLGA NCs would reflect similarly efficient targeting and transport to destination as well, given a similar enzyme load per NC. As for polystyrene models, PLGA nanoparticles (obtained by nanoprecipitation and solvent evaporation, as reported [24,26,30]) had average diameter of 155 nm in diameter and PDI of 0.08, with a slightly more negative  $\zeta$ -potential (-48 mV), as expected for PLGA (Table 1). Coating with  $\gamma$ 3 and ASM resulted in a similar increase in size to that experienced by polystyrene models, resulting in a preparation with average size of 266 nm in diameter and 0.12 PDI, and a less negative  $\zeta$ -potential (-30 mV). The enzyme loading efficiency and absolute loading per NC were also similar to polystyrene models (94% efficiency; 251 ASM molecules per NC). Finally,  $\gamma$ 3/ASM PLGA NCs showed similar reduction of lysosomal sphingomyelin and cholesterol storage than polystyrene models, i.e. 96.3% and 94.8% reduction, respectively,  $\approx$ 100% the same efficacy as  $\gamma$ 3/ASM polystyrene NCs.

### Discussion

Previous studies using polymer NCs coated with anti-ICAM antibody molecules have illustrated great promise of this strategy to improve the delivery of recombinant enzymes

used for enzyme replacement therapy of LDs [7-9,24,25]. Nevertheless, further evaluation of the translational potential of this strategy will require optimization of these formulations to maximize their biocompatibility. This is of major relevance, since the LDs are chronic conditions and enzyme replacement therapy is implemented to treat, not cure, patients [1,3]. In this regard, the use of short targeting peptides likely to be more “invisible” to the immune system, instead of antibodies or their fragments, is interesting since this may help minimize potential side effects of treatment.

The goal of this study was to examine for the first time if polymer NCs coated with a non-antibody, ICAM-1-targeting peptide hold promise to enhance delivery of recombinant enzymes to lysosomal compartments, for reduction of the aberrant lysosomal storage characteristic of LDs. In particular, the peptide we used, known as  $\gamma 3$ , is derived from the sequence of fibrinogen, a protein abundant in circulation which binds to ICAM-1 and other cell-surface markers in pro-thrombotic/inflammatory conditions [29]. The  $\gamma 3$  sequence is specific for ICAM-1, as shown previously and verified here in the context of NC targeting (Figures 1 and 2). Our results further demonstrate that peptide-coated NCs bearing recombinant lysosomal enzymes (illustrated in the case of ASM) effectively bind to ICAM-1 on cells (Figures 1-3), are internalized via the CAM-mediated route (Figure 4), traffic to lysosomes (Figure 5), and restore degradation of lysosomal substrates (sphingomyelin and cholesterol) otherwise aberrantly stored in disease cells (Figure 6).

A previous work from our group showed that  $\gamma 3$  held potential to substitute anti-ICAM as a targeting moiety for NC targeting and uptake [32], yet the implementation of these NCs to effectively deliver a therapeutic cargo rendering functional activity had not been determined. Although one would expect that a cargo would not greatly compromise the binding and transport properties of a targeted NC, one cannot disregard an effect on this line. For the reasons already described in the introduction, NC surface-loading of lysosomal enzymes is reasonable. However, ASM (as other lysosomal enzymes) displays M6P residues [2,35] which may compete for binding to the M6P receptor expressed on most cells, and uptake via the M6P receptor has been shown to be altered in NPD [36,37]. Under this scenario, that fact that  $\gamma 3$  NCs bound well to cells did not guarantee that  $\gamma 3$ /ASM NCs would, as the presence of ASM on  $\gamma 3$  NCs may have obliterated the delivery improvement originally intended. Luckily, comparison of the data obtained in this study for  $\gamma 3$ /ASM NCs to our previous publication on  $\gamma 3$  NCs suggests that all processes, including binding, endocytosis, and lysosomal transport were similar for both formulations. The fact that an anti-ICAM antibody (not M6P) competed off the binding of  $\gamma 3$ /ASM NCs to cells (Figure 2) further verifies that ASM cargo did not impact the intended targeting.

Also important is the fact that  $\gamma 3$ /ASM NCs performed with efficiency similar to anti-ICAM/ASM NCs [32], as shown in Figures 2 with regard to binding to target cells and Figure 3 on lysosomal trafficking. Moreover, comparison of the functional activity of  $\gamma 3$ /ASM NCs with anti-ICAM counterparts (Figure 6B), significantly strengthens the conclusion that this more biocompatible iteration of our ICAM-1 targeting strategy is promising and worth of further examination and development.

The literature has described several non-antibody affinity peptides capable of selective binding to ICAM-1, including peptides identified by phage display or derived from the sequence of proteins that can bind to ICAM-1, such as MUC1 mucin core proteins, P(0) CAM, leukocyte functional antigen-1 (LFA-1), and others [38-42]. These peptides were designed and tested mostly in the context of blocking ICAM-1-mediated inflammation and/or cancer metastasis, and some of them also showed potential for use in drug delivery and imaging [20,21-42,43]. However, most of these peptides were specifically designed to target human ICAM-1 and their species cross-reactivity for use in laboratory animals is unknown. The animal model for NPD is the ASM knockout mouse [35] and mice constitute the most common and available tool for *in vivo* studies for majority of LDs [4]. Since pre-clinical development of lysosomal enzyme replacement therapy is largely based upon mouse models, the use of targeting moieties which recognize receptors in multiple species is critical. As shown here,  $\gamma 3$ /ASM NCs had the ability to target both mouse and human ICAM-1 (Figure 3) and lysosomal transport was found in both scenarios (Figure 5). Therefore, our next focus will be on examining the targeting and therapeutic potential of  $\gamma 3$ /ASM NCs in the ASM knockout mouse continue developing this strategy.

In addition, most previous ICAM-1-targeting peptides have not been studied in the context of defining their ability to induce endocytosis via the CAM route followed by lysosomal trafficking, key for this application. Noteworthy, not all affinity molecules designed to bind to the same cell-surface marker have the ability to induce endocytic transport and lysosomal trafficking. For example, previous studies using the model NCs used here, coated with antibodies against PECAM-1 (another adhesion molecule internalized via CAM-mediated endocytosis), revealed that targeting each of three different epitopes located on the same domain, of the same receptor, on the same type of cells, lead to three different cellular responses despite NC binding being similar [27]. NCs coated with one antibody bound but did not enter cells, NCs coated with a second antibody induced uptake and lysosomal transport, and NCs coated with a third antibody enter cells but did not traffic to this compartment [27]. This illustrates that, as documented for this endocytic route, NC binding is not enough to achieve efficient uptake or lysosomal delivery. Whether other ICAM-1 targeting peptides would result in a similar behavior remains to be explored.

Interestingly, despite its abundance in blood, fibrinogen does not bind to endothelial ICAM-1 under control conditions, but pro-inflammatory activation of the endothelium prompts the interaction of this molecule with multiple endothelial cell-surface markers [10,44]. Under such inflammatory state, the particular binding of fibrinogen to ICAM-1 strengthens the interaction between endothelial cells and macrophages in inflammation [44]. Therefore, the  $\gamma 3$  peptide is expected to preferentially bind to endothelial cells activated under pathological states (as we have previously demonstrated) and, perhaps, this may block or weaken macrophage-endothelial attachment in this context, as shown for the soluble peptide [29]. Given that inflammation develops and contributes significantly to the progression and response to treatment of LDs [1,4], this would represent a secondary benefit of using this targeting strategy. As an example, our recent study using anti-ICAM NCs indicated that since ICAM-1 is endocytosed bound to anti-ICAM NCs, this temporarily removes ICAM-1 from the endothelial surface and, in turn, reduces the levels of soluble ICAM-1 released by endothelial cells [45]. Soluble ICAM-1 has been shown to be generated

upon cleavage of membrane-expressed ICAM-1 and is a pro-inflammatory mediator [46]. By lowering this factor, ICAM-1-targeted NCs may offer additional advantages.

## Conclusions

The results of this study demonstrate that substitution of anti-ICAM molecules by a more biocompatible targeting moiety, the fibrinogen-derived peptide  $\gamma 3$ , on the coat of polymer NCs is a viable strategy to provide targeting, endocytosis, lysosomal delivery, and effects of recombinant lysosomal enzymes used for replacement therapy of LDs. Our future studies will focus on examining the potential of this new formulation in animal models, to tune therapeutic delivery and potential side effects toward pre-clinical development.

## Acknowledgments

The authors thank Dr. Edward Schuchman (Department of Genetics and Genomic Sciences, Mount Sinai School of Medicine, New York, NY) for providing recombinant human ASM and NPD fibroblasts, and Dr. Melani Solomon and Mr. Niksa Roki (Fischell Department of Bioengineering, University of Maryland, College Park, MD) for technical assistance. This work was supported by National Institutes of Health award R01-HL98416 and National Science Foundation award CBET-1402756 (to S.M.).

## References

1. Parenti G, Andria G, Ballabio A. Lysosomal storage diseases: from pathophysiology to therapy. *Ann Rev Med.* 2015; 66:471–486. [PubMed: 25587658]
2. Futerman AH, van Meer G. The cell biology of lysosomal storage disorders. *Nat Rev Mol Cell Biol.* 2004; 5:554–565. [PubMed: 15232573]
3. Parkinson-Lawrence EJ, Shandala T, Prodoehl M, et al. Lysosomal storage disease: revealing lysosomal function and physiology. *Physiol.* 2010; 25:102–115.
4. Solomon M, Muro S. Lysosomal enzyme replacement therapies: historical development, clinical outcomes, and future perspectives. *Adv Drug Deliv Rev.* 2017 Accepted with minor revision.
5. Kirkegaard T. Emerging therapies and therapeutic concepts for lysosomal storage diseases. *Expert Opin Orphan Drugs.* 2013; 1:385–404.
6. Muro S. Strategies for delivery of therapeutics into the central nervous system for treatment of lysosomal storage disorders. *Drug DelivTransl Res.* 2012; 2:169–186.
7. Hsu J, Northrup L, Bhowmick T, et al. Delivery of  $\alpha$ -glucosidase for Pompe disease by ICAM-1-targeted polymer nanocarriers. *Nanomed.* 2012; 8:731–739.
8. Hsu J, Serrano D, Bhowmick T, Kumar K, et al. Enhanced endothelial delivery and biochemical effects of  $\alpha$ -galactosidase by ICAM-1-targeted nanocarriers for Fabry disease. *J Control Rel.* 2011; 149:323–331.
9. Garnacho C, Dhami R, Simone E, et al. Delivery of acid sphingomyelinase in normal and Niemann-Pick disease mice using ICAM-1-targeted polymer nanocarriers. *J Pharm ExpTher.* 2008; 325:400–408.
10. Muro, S. Intercellular adhesion molecule-1 and vascular cell adhesion molecule-1. In: Aird, W., editor. *Endothelial biomedicine.* Cambridge University Press; New York, NY: 2007. p. 1058-1070. Chapter 117
11. Muro S, Wiewrodt R, Thomas A, et al. A novel endocytic pathway induced by clustering endothelial ICAM-1 or PECAM-1. *J Cell Sci.* 2003; 116:1599–1609. [PubMed: 12640043]
12. Serrano D, Bhowmick T, Chadha R, et al. Intercellular adhesion molecule 1 engagement modulates sphingomyelinase and ceramide, supporting uptake of drug carriers by the vascular endothelium. *ArteriosclerThrombVasc Biol.* 2012; 32(5):1178–1185.
13. Rappaport J, Manthe R, Solomon M, et al. A Comparative study on the alterations of endocytic pathways in multiple lysosomal storage disorders. *Mol Pharm.* 2016; 13:357–368. [PubMed: 26702793]

14. Serrano, D., Muro, S. Endothelial cell adhesion molecules and drug delivery applications. In: Aranda-Espinoza, H., editor. *Mechanobiology of the endothelium*. CRC Press; Boca Raton, USA: 2014. p. 185-226. Chapter 9
15. Muro S. A DNA device that mediates selective endosomal escape and intracellular delivery of drugs and biological. *AdvFunct Mat*. 2014; 24:2899–2906.
16. Choi KS, Kim SH, Cai QY, et al. Inflammation-specific T1 imaging using anti-intercellular adhesion molecule 1 antibody-conjugated gadolinium diethylenetriaminepentaacetic acid. *Mol Imaging*. 2007; 6:75–84. [PubMed: 17445502]
17. Weller GE, Villanueva FS, Tom EM, et al. Targeted ultrasound contrast agents: in vitro assessment of endothelial dysfunction and multi-targeting to ICAM-1 and sialyl Lewisx. *Biotechnol Bioeng*. 2005; 92:780–788. [PubMed: 16121392]
18. Greineder CF, Chacko AM, Zaytsev S, et al. Vascular immunotargeting to endothelial determinant ICAM-1 enables optimal partnering of recombinant scFv-thrombomodulin fusion with endogenous cofactor. *PLoS One*. 2013; 8:e80110. [PubMed: 24244621]
19. Mastrobattista E, Storm G, van Bloois L, et al. Cellular uptake of liposomes targeted to intercellular adhesion molecule-1 (ICAM-1) on bronchial epithelial cells. *Biochim Biophys Acta*. 1999; 1419:353–363. [PubMed: 10407086]
20. Zhang N, Chittasupho C, Duangrat C, et al. PLGA nanoparticle-peptide conjugate effectively targets intercellular cell-adhesion molecule-1. *Bioconjug Chem*. 2008; 19:145–152. [PubMed: 17997512]
21. Park S, Kang S, Veach AJ, et al. Self-assembled nanoplatform for targeted delivery of chemotherapy agents via affinity-regulated molecular interactions. *Biomaterials*. 2010; 31:7766–7775. [PubMed: 20667589]
22. Anselmo AC, Gupta V, Zern BJ, et al. Delivering nanoparticles to lungs while avoiding liver and spleen through adsorption on red blood cells. *ACS Nano*. 2013; 7:11129–11137. [PubMed: 24182189]
23. Shuvaev VV, Ilies MA, Simone E, et al. Endothelial targeting of antibody-decorated polymeric filomicelles. *ACS Nano*. 2011; 5:6991–6999. [PubMed: 21838300]
24. Muro S, Schuchman E, Muzykantov V. Lysosomal enzyme delivery by ICAM-1 targeted nanocarriers bypassing glycosylation- and clathrin-dependent endocytosis. *MolTher*. 2006; 13:135–141.
25. Hsu J, Bhowmick T, Burks S, et al. Enhancing biodistribution of therapeutic enzymes in vivo by modulating surface coating and concentration of ICAM-1-targeted nanocarriers. *J Biomed Nanotech*. 2013; 10:345–354.
26. Muro S, Dziubla T, Qiu W, et al. Endothelial targeting of high-affinity multivalent polymer nanocarriers directed to ICAM-1. *J Pharm ExpTher*. 2006; 317:1161–1169.
27. Garnacho C, Albelda S, Muzykantov V, et al. Differential intra-endothelial delivery of polymer nanocarriers targeted to distinct PECAM-1 epitopes. *J Control Rel*. 2008; 130:226–233.
28. Han J, Shuvaev VV, Davies PF, et al. Flow shear stress differentially regulates endothelial uptake of nanocarriers targeted to distinct epitopes of PECAM-1. *J Control Rel*. 2015; 28:39–47.
29. Altieri DC, Duperray A, Plescia J, et al. Structural recognition of a novel fibrinogen gamma chain sequence (117-133) by intercellular adhesion molecule-1 mediates leukocyte-endothelium interaction. *J Biol Chem*. 1995; 270:696–699. [PubMed: 7822297]
30. Ghaffarian R, Pérez-Herrero E, Oh H, et al. Chitosan-alginate microcapsules provide gastric protection and intestinal release of ICAM-1-targeting nanocarriers, enabling GI targeting in vivo. *Adv Func Mat*. 2016; 26:3382–3393.
31. Serrano D, Manthe RL, Paul E, et al. How Carrier Size and Valency Modulate Receptor-Mediated Signaling: Understanding the Link between Binding and Endocytosis of ICAM-1-Targeted Carriers. *Biomacromolecules*. 2016; 17:3127–3137. [PubMed: 27585187]
32. Garnacho C, Serrano D, Muro S. A fibrinogen-derived peptide provides ICAM-1-specific vascular targeting and intra-endothelial transport of polymers nanocarriers in cell cultures and mice. *J Pharm ExpTher*. 2012; 340:638–647.

33. Muro S, Cui X, Gajewski CM, et al. Slow intracellular trafficking of catalase nanoparticles targeted to ICAM-1 protects endothelial cells from oxidative stress. *Am J Phys-Cell Physiology*. 2003; 285:C1339–13347.
34. Muro S, Garnacho C, Champion J, et al. Controlled endothelial targeting and intracellular delivery of therapeutics by modulating size and shape of ICAM-1-targeted carriers. *MolTher*. 2008; 16:1450–1458.
35. Schuchman EH. The pathogenesis and treatment of acid sphingomyelinase-deficient Niemann-Pick disease. *J Inherit Metab Dis*. 2007; 30:654–663. [PubMed: 17632693]
36. Rappaport J, Garnacho C, Muro S. Clathrin-mediated endocytosis is impaired in type A-B Niemann-Pick disease model cells and can be restored by ICAM-1-mediated enzyme replacement. *Mol Pharm*. 2014; 11:2887–2895. [PubMed: 24949999]
37. Dhimi R, Schuchman EH. Mannose 6-phosphate receptor-mediated uptake is defective in acid sphingomyelinase-deficient macrophages: implications for Niemann-Pick disease enzyme replacement therapy. *J Biol Chem*. 2004; 279:1526–1532. [PubMed: 14557264]
38. Belizaire AK, Tchistiakova L, St-Pierre Y, et al. Identification of a murine ICAM-1-specific peptide by subtractive phage library selection on cells. *Biochem Biophys Res Commun*. 2003; 309:625–630. [PubMed: 12963036]
39. Anderson ME, Siahaan TJ. Mechanism of binding and internalization of ICAM-1-derived cyclic peptides by LFA-1 on the surface of T cells: a potential method for targeted drug delivery. *Pharm Res*. 2003; 20:1523–1532. [PubMed: 14620502]
40. Sillerud LO, Burks EJ, Brown WM, et al. NMR solution structure of a potent cyclic nonapeptide inhibitor of ICAM-1-mediated leukocyte adhesion produced by homologous amino acid substitution. *J Pept Res*. 2004; 64:127–140. [PubMed: 15357668]
41. Welply JK, Steininger CN, Caparon M, et al. A peptide isolated by phage display binds to ICAM-1 and inhibits binding to LFA-1. *Proteins*. 1996; 26:262–270. [PubMed: 8953648]
42. Khodabandehlou K, Masehi-Lano JJ, Poon C, et al. Targeting cell adhesion molecules with nanoparticles using in vivo and flow-based in vitro models of atherosclerosis. *ExpBiol Med*. 2017; 242:799–812.
43. Chittasupho C, Xie SX, Baoum A, et al. ICAM-1 targeting of doxorubicin-loaded PLGA nanoparticles to lung epithelial cells. *Eur J Pharm Sci*. 2009; 37:141–150. [PubMed: 19429421]
44. Languino LR, Plescia J, Duperray A, et al. Fibrinogen mediates leukocyte adhesion to vascular endothelium through an ICAM-1-dependent pathway. *Cell*. 1993; 73:1423–1434. [PubMed: 8100742]
45. Manthe R, Muro S. ICAM-1-targeted nanocarriers attenuate endothelial release of sICAM-1, and inflammatory regulator. *Bioeng Transl Med*. 2017; In press. doi: 10.1002/btm2.10050
46. Witkowska AM, Borawska MH. Soluble intercellular adhesion molecule-1 (sICAM-1): an overview. *Eur Cytokine Netw*. 2004; 15:91–98. [PubMed: 15319166]

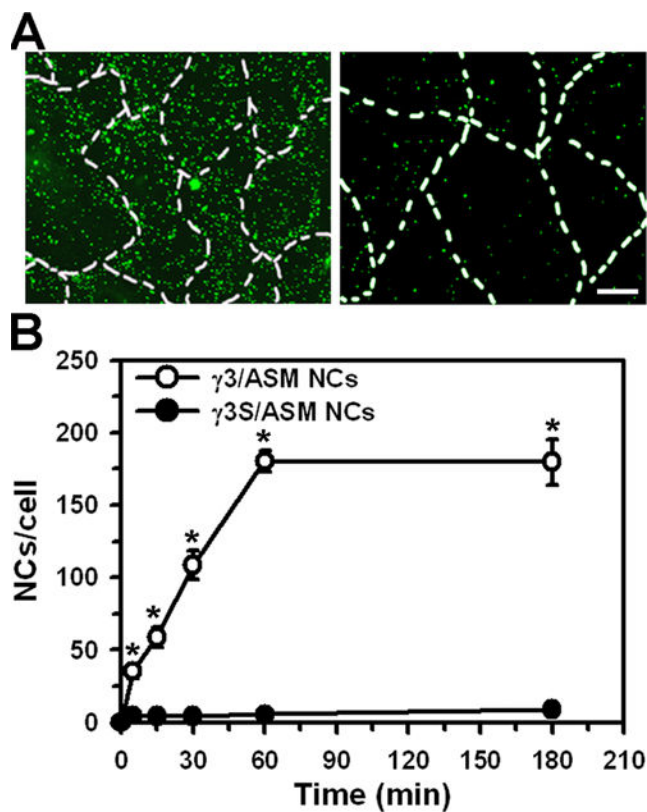


**Figure 1. Specificity and binding kinetics of  $\gamma3$ /ASM NCs to endothelial cells**  
(A) TNF $\alpha$ -activated, fixed HUVECs incubated for 1 h at 37°C with model, green Fluoresbrite®-polystyrene NCs coated with ASM enzyme cargo and ICAM-1-targeted, fibrinogen-derived  $\gamma3$ peptide vs. non-specific scrambled-sequence peptide ( $\gamma3S$ ). Dashed lines mark cell borders, determined by phase-contrast. Scale bar: 10  $\mu$ m. (B) The number of NCs bound per cell between 5 min to 3 h was quantified from fluorescence images. Data are mean  $\pm$  SEM. \*Compares  $\gamma3$ /ASM NCs to  $\gamma3S$ /ASM NCs;  $p < 0.01$ , by Student's  $t$ -test.

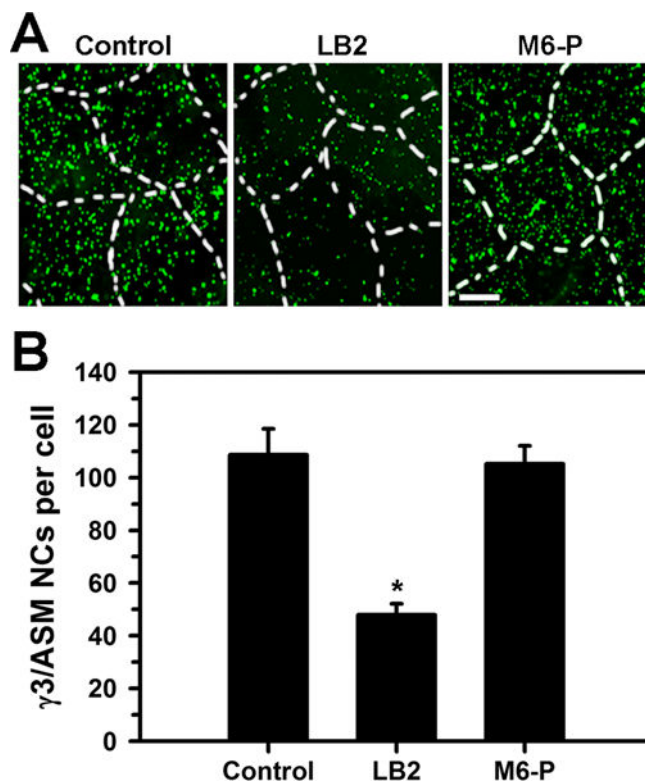


**Figure 2. ICAM-1, not M6P, targeting of  $\gamma$ 3/ASM NCs**

(A) TNF $\alpha$ -activated HUVECs incubated for 30 min at 37°C with green Fluoresbrite®-polystyrene NCs coated with ASM and  $\gamma$ 3, in the absence (Control) vs. presence of competing “ligands” against: ICAM-1 (antibody LB2) or the M6P receptor (mannose-6-phosphate, M6P). Dashed lines mark cell borders, determined by phase-contrast. Scale bar: 10  $\mu$ m. (B) The number of NCs bound per cell was quantified from fluorescence images. Data are mean  $\pm$  SEM. \*Compares against control;  $p < 0.01$ , by Student’s  $t$ -test.

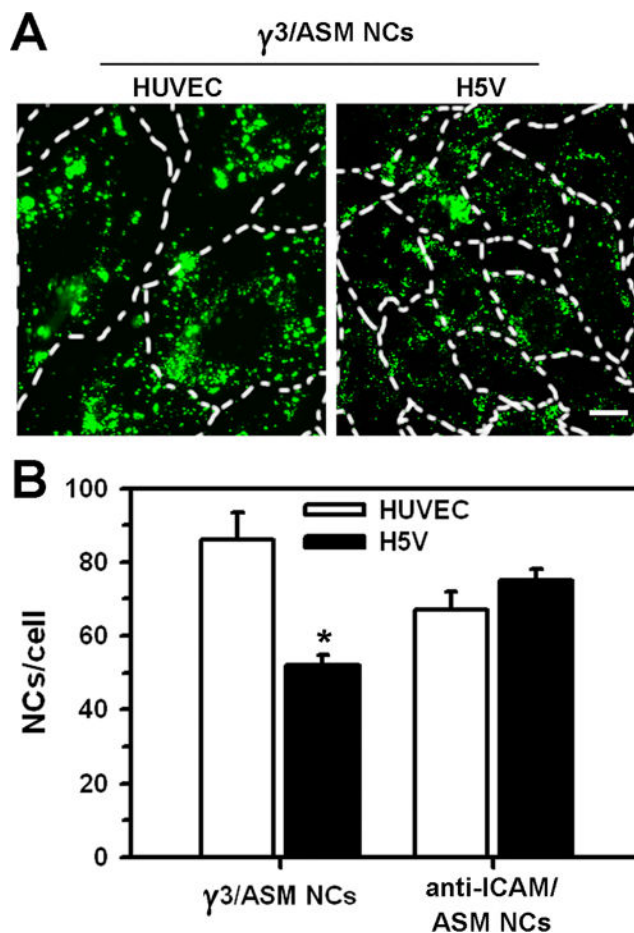


**Figure 3. Comparison of peptide vs. antibody targeted ASM NCs in human and mouse endothelial cells**

(A) TNF $\alpha$ -activated human vs. mouse endothelial cells (HUVECs vs. H5V, respectively), incubated for 1 hat 37°C with green Fluoresbrite®-polystyrene NCs coated with  $\gamma$ 3 and ASM. Dashed lines mark cell borders, determined by phase-contrast. Scale bar: 10  $\mu$ m. (B) The number of NCs bound per cell was quantified from fluorescence images in (A) and compared to antibody-targeted anti-ICAM/ASM NCs. Data are mean  $\pm$  SEM. \*Compares H5V vs. HUVEC;  $p < 0.01$ , by Student's  $t$ -test. No difference was observed between peptide- and antibody-coated counterparts.

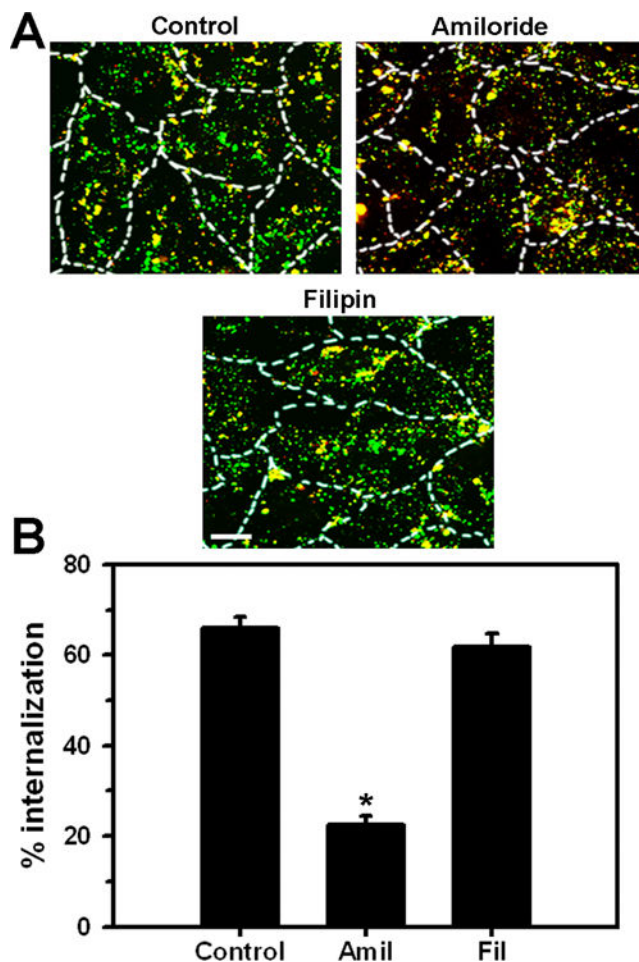


**Figure 4. Mechanism of endocytosis of  $\gamma$ 3/ASM NCs**

(A) TNF $\alpha$ -activated HUVECs incubated for 1 h pulse at 37°C with green Fluoresbrite®-polystyrene NCs coated with  $\gamma$ 3 and ASM, in the absence (Control) vs. presence of the inhibitors of CAM-mediated vs. caveolar-mediated endocytosis, amiloride (Amil) vs. filipin (Fil). Cells were washed and incubated for 1 h chase in NC-free medium containing or not inhibitors. NCs contained a tracer of non-specific IgG on their surface to enable differential staining of cell-bound but not internalized NCs with a Texas Red-labeled secondary antibody. Therefore, internalized NCs appear single-labeled in green vs. cell-surface bound NCs which appear double-labeled (green + red) as yellow. Dashed lines mark cell borders, determined by phase-contrast. Scale bar: 10  $\mu$ m. (B) The percentage of all cell-associated NCs that were internalized was quantified from fluorescence images. Data are mean  $\pm$  SEM. \*Compares against Control;  $p < 0.01$ , by Student's  $t$ -test.

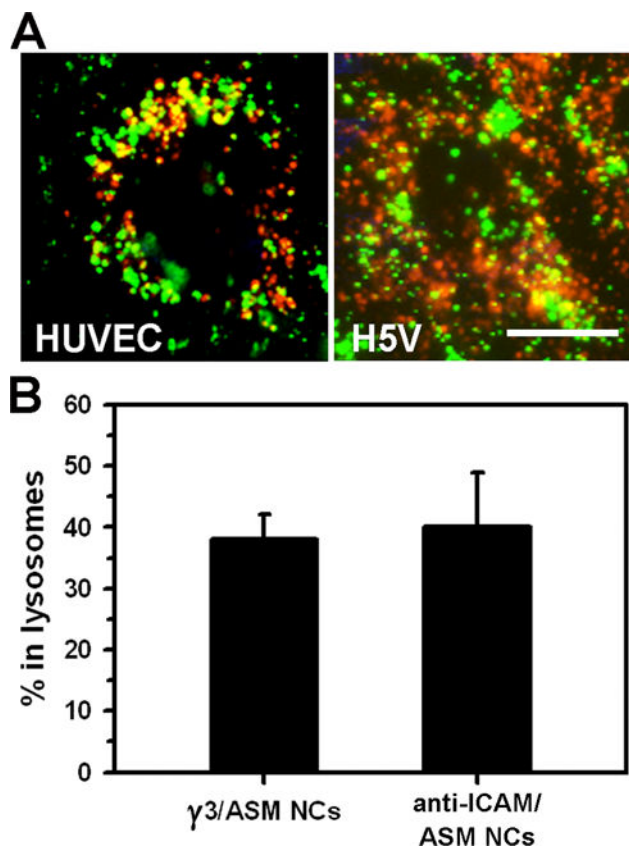


**Figure 5. Lysosomal colocalization of  $\gamma 3$ /ASM NCs vs. anti-ICAM/ASM NCs**  
(A) TNF $\alpha$ -activated HUVECs or H5V cells were incubated for 1 h at 37°C with Texas Red dextran to label lysosomes, followed by washing and incubation of cells with green Fluoresbrite®-polystyrene NCs coated with ASM and  $\gamma 3$  for 1 h at 37°C to allow binding and uptake (pulse). After washing, cells were incubated for 2 h more (chase), and then fixed. Fluorescence microscopy images show green NCs that do not colocalize with red lysosomes vs. lysosomal-located NCs which appear yellow (green+red). Dashed lines mark cell borders, determined by phase-contrast. Scale bar: 10  $\mu$ m. (B) The percentage of internalized NCs that colocalized with lysosomes was quantified from HUVECs fluorescence images and compared to anti-ICAM/ASM NCs. Data are mean  $\pm$  SEM. No statistical difference was observed between polystyrene model and PLGA NCs.

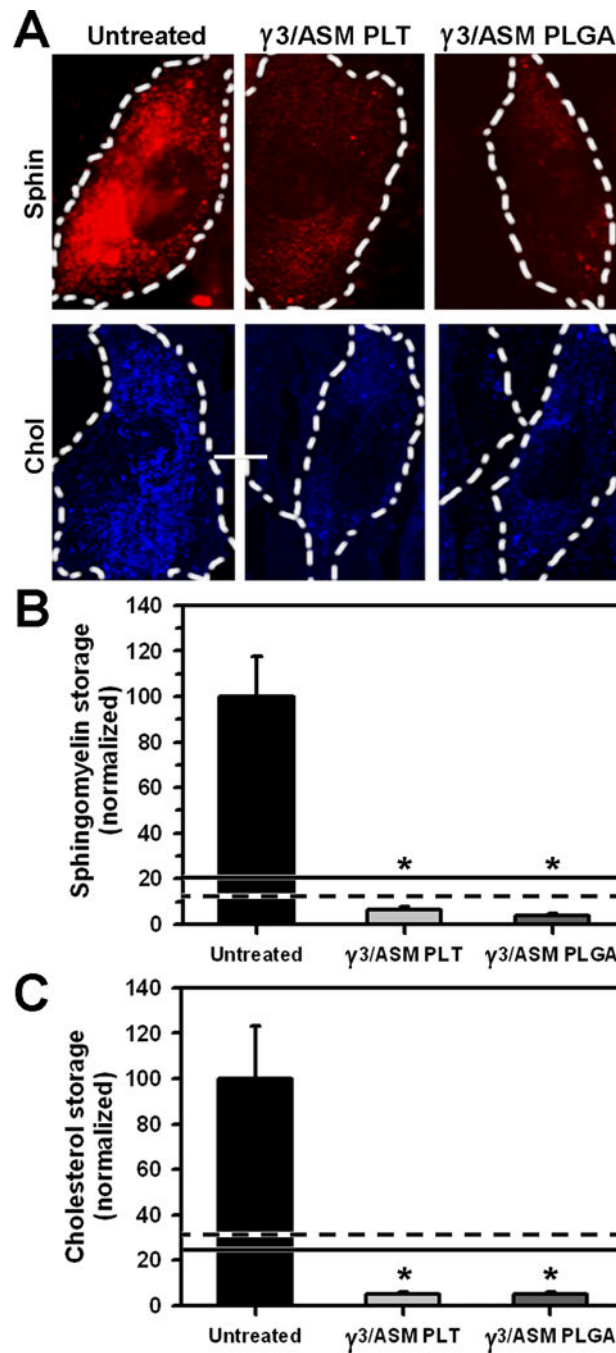


**Figure 6. Therapeutic activity of ASM delivered by  $\gamma 3$ -targeted polystyrene and PLGA NCs** (A) Skin fibroblasts from an NPD patient or a normal (wild type) individual were incubated overnight with red-fluorescent BODIPY-FL<sub>C12</sub>-sphingomyelin to label lysosomal storage of this lipid. After washing, cells were incubated at 37°C for 1 h binding pulse with control medium (Untreated) or medium containing polystyrene vs. PLGA NCs, both coated with ASM and  $\gamma 3$ . Cells were washed and incubated for 5 h in NC-free medium, then fixed. Cholesterol was then stained blue with filipin. Dashed lines mark cell borders, determined by phase-contrast. Scale bar: 10  $\mu$ m. (B) The level of sphingomyelin and (C) cholesterol

storage were analyzed from fluorescence micrographs and expressed as a percentage of untreated cells. (B-C) Solid line = lipid levels for normal cells. Dashed line = lipid levels after treatment with anti-ICAM/ASM NCs. Data are mean  $\pm$  SEM. \*Compares NC treatment against untreated cells;  $p < 0.01$ , by Student's *t*-test. No differences were found between polystyrene and PLGA NCs.

Author Manuscript

Author Manuscript

Author Manuscript

Author Manuscript

Table 1

NC characterization.

Formulation	Size (nm)	PDI	Z potential (mV)	% Efficiency (coated/added)	ASM(molecules/NC)
<i>Polystyrene models</i>					
Non-coated NCs	117.2 ± 2.0	0.07 ± 2.0	-36.7 ± 2.0	—	—
γ3/ASM NCs	209.5 ± 8.4	0.14 ± 2.0	-25.3 ± 0.5	79.7 ± 14.1	211.7 ± 37.4
γ3S/ASM NCs	205.0 ± 29.2	0.19 ± 2.0	—	—	—
Anti-ICAM/ASM NCs	216.2 ± 17.1	0.14 ± 2.0	-27.3 ± 0.9	85.0 ± 15.4	236.2 ± 17.3
<i>PLGA NCs</i>					
Non-coated NCs	154.8 ± 2.0	0.08 ± 0.01	-48.3 ± 4.1	—	—
γ3/ASM NCs	265.8 ± 30.8	0.12 ± 0.02	-30.5 ± 0.3	94.5 ± 3.1	251.0 ± 8.2

Average values for n = 3 independent preparations are shown.